



HAL
open science

Influence of divalent cations in the protein crystallization process assisted by lanthanide-based additives

Amandine Roux, Romain Talon, Zaynab Alsalman, Sylvain Engilberge, Anthony d' Aléo, Sebastiano Di Pietro, Adeline Robin, Alessio Bartocci, Guillaume Pilet, Elise Dumont, et al.

► To cite this version:

Amandine Roux, Romain Talon, Zaynab Alsalman, Sylvain Engilberge, Anthony d' Aléo, et al.. Influence of divalent cations in the protein crystallization process assisted by lanthanide-based additives. *Inorganic Chemistry*, 2021, 60 (20), pp.15208-15214. 10.1021/acs.inorgchem.1c01635 . hal-03407486

HAL Id: hal-03407486

<https://hal.science/hal-03407486v1>

Submitted on 28 Oct 2021

HAL is a multi-disciplinary open access archive for the deposit and dissemination of scientific research documents, whether they are published or not. The documents may come from teaching and research institutions in France or abroad, or from public or private research centers.

L'archive ouverte pluridisciplinaire **HAL**, est destinée au dépôt et à la diffusion de documents scientifiques de niveau recherche, publiés ou non, émanant des établissements d'enseignement et de recherche français ou étrangers, des laboratoires publics ou privés.

Influence of divalent cations in the protein crystallisation process assisted by Lanthanide-based additives.

Amandine Roux,^{†,‡} Romain Talon,[□] Zaynab Alsalman,[□] Sylvain Engilberge,[□] Anthony D'Aléo,[†] Sebastiano Di Pietro,[†] Adeline Y. Robin,[□] Alessio Bartocci,[†] Guillaume Pilet,[≠] Elise Dumont,^{†,□} Tristan Wagner,^{§,¥} Seigo Shima,[§] François Riobé,^{†*} Eric Girard,^{□*} Olivier Maury^{†*}

[†] Univ Lyon, ENS de Lyon, CNRS UMR 5182, Laboratoire de Chimie, F-69342 Lyon, France. E-mail: olivier.maury@ens-lyon.fr, francois.riobe@ens-lyon.fr,

[‡] Polyvalan Company, F-69342 Lyon, France.

[□] Univ Grenoble Alpes, CEA, CNRS, IBS, F-38000 Grenoble, France. E-mail: eric.girard@ibs.fr.

[≠] Univ de Lyon, CNRS UMR 5615, Université Claude Bernard Lyon 1, 43 boulevard du 11 novembre 1918, F-69622 Villeurbanne cedex.

[□] Institut Universitaire de France, 1 rue Descartes, 75005 Paris

[§] Microbial Protein Structure Group, Max Planck Institute for Terrestrial Microbiology, Karl-von-Frisch-Str. 10, D-35043 Marburg, Germany

[¥] Microbial Metabolism Group, Max Planck Institute for Marine Microbiology, 1-Celsiusstrasse, 35043 Bremen, Germany

Supporting Information Placeholder

ABSTRACT Lanthanide complexes are now widely used as powerful auxiliaries for protein crystallisation to improve the crucial nucleation and phasing steps. We systematically analysed the influence of the commercial crystallisation kit composition on the efficiency of two lanthanide additives [Na]₃[Eu(DPA)₃] and Tb-Xo4, we developed. This study revealed that our initial the tris-dipicolinate complex presents a lower chemical stability and a strong tendency to self-crystallisation detrimental for its use in high-throughput robotised crystallisation platform. In particular, we reported herein the crystal structures of (Mg(H₂O)₆)₃[Eu(DPA)₃]₂·7H₂O (**1**), {(Ca(H₂O)₄)₃[Eu(DPA)₃]₂}_n·11nH₂O (**2**) and {Cu(DPA)(H₂O)₂}_n (**3**) resulting from spontaneous crystallisation in the presence of divalent alkaline earth cation or transmetalation. On the other hand, the Tb-Xo4 is perfectly soluble in the crystallisation media, stable in the presence of alkaline-earth dications and slowly decomposed (within days) by trans-metalation with transition metals. The original structure of [Tb₄L₄(H₂O)₄]Cl₄·15H₂O (**4**) is also described. In this article, we also discussed the potential beneficial interactions between the crystallisation mixture components and Tb-Xo4 leading to the formation of more complex adducts observed in the case of the AdKA protein crystallisation, like {AdkA/Tb-Xo4/Mg²⁺/glycerol} in the protein binding sites. The observation of such multi-components adducts illustrates the complexity and the versatility of the supramolecular chemistry occurring at the surface of proteins.

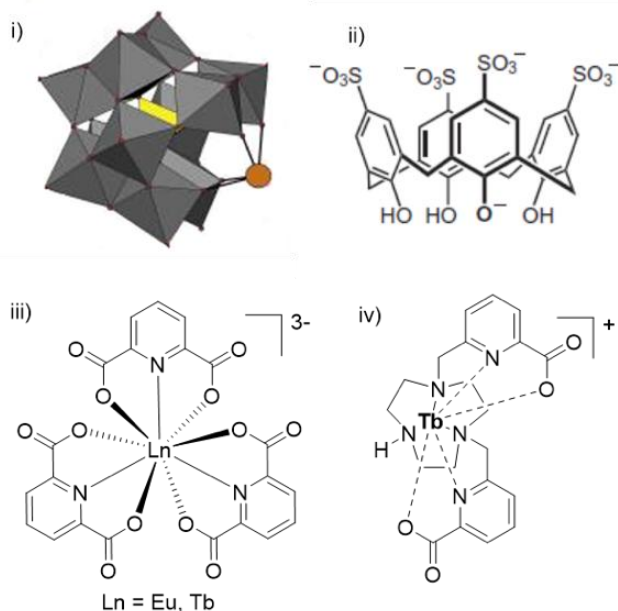
Introduction

Over the past decade, the number of X-rays protein structures deposited in the Protein Data Bank (PDB <https://www.rcsb.org/>) has increased steadily despite the emergence of alternative techniques, such as NMR or cryoEM. Almost 90 % of new-deposited structures are still elucidated using X-ray crystallography. However, this last method still suffers from two major chokepoints that have a great impact on its efficiency : i) the production of high-quality single crystals and ii) the phase determination which is mandatory for electron density map calculation.¹⁻² The structural genomics statistics actually estimates that only 10% of the purified proteins will see their structure solved, consequently leaving a considerable room for improvement in the protein biochemistry and protein crystallisation fields.³ To tackle these drawbacks, the main stream developments are concentrated in

the field of technology: improvement of structure determination pipelines, building of more intense radiation sources or use of XFEL source to address even smaller crystals, and use of high-throughput crystallisation platforms to screen an even larger number of conditions with a reduced amount of purified protein sample.⁴⁻⁵ Unfortunately, the certain success of these developments leads, in comparison, to neglect the traditional methodological approaches, in particular, the research for low-cost additives that can either stimulate the crystallisation or solve the phase determination problems or even better both simultaneously.

Indeed, it is well known that incorporation in a protein crystal of well-ordered heavy atom enable the solution of the phase problem using anomalous-based methods – Single-wavelength Anomalous Dispersion (SAD) and Multi-wavelength Anomalous Dispersion (MAD).⁶ These heavy atoms can be

introduced in a covalent way as pioneered by the Doublé's S-to-Se replacement using selenomethionine or in a non-covalent way using lanthanide complexes.⁷ On the other hand, the development of additives that facilitate the nucleation process was initially focused on heterogeneous compounds like minerals, natural materials such as horse and human hair, nano-porous materials⁸⁻⁹ and more recently molecular imprinted polymers.¹⁰⁻¹¹ However, these solid additives are



hardly compatible with the widely-used homogeneous high-throughput crystallisation methods.

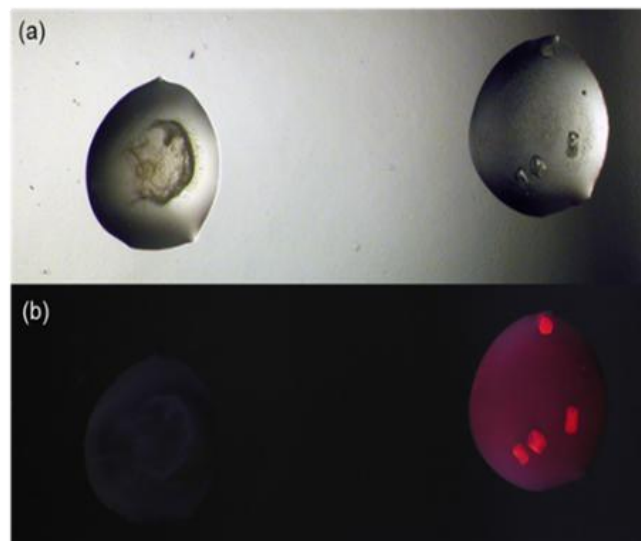
Figure 1. Selected examples of the three families of soluble additives used in protein crystallography. (i) Keggin polyoxometalate structure of $[\text{Ce}(\alpha\text{-PW}_{11}\text{O}_{39})_2]^{10-}$, (ii) p-sulfonatocalix[4]arene (slx4) and lanthanide derivatives studied in this work (iii) tris-dipicolinate $[\text{Na}]_3[\text{Ln}(\text{DPA})_3]$ and (iv) crystallophore (Tb-Xo4).

Recently, new soluble additives were developed that are fully compatible with the automated crystallisation screening systems (Figure 1): i) the polyoxo-metalates developed by Rompel and co-workers,¹²⁻¹⁵ ii) the anionic or neutral macrocycles proposed by the team of Crowley (phosphonated or sulfonato-calix[4,6,8]arenes, and cucurbituryls...),¹⁶⁻¹⁹ and the lanthanide complexes (iii) tris-dipicolinate²⁰⁻²¹ and iv) crystallophore (Tb-Xo4),²² developed by our group. All these species can be considered as “molecular glues” inducing a network of supramolecular interactions with proteins in solution, favoring nucleation and crystalline contacts in the packing. Among these three families of additives, polyoxometalate and lanthanide complexes contain heavy atoms (tungsten, europium or terbium, respectively) and can therefore solve simultaneously the nucleating and the phase determination issues. In particular, based on our own statistics obtained on twenty proteins, the crystallophore increases the number of crystallisation hits by a factor 3-to-7, gives better quality crystals generally suppressing twinning issue and enables de novo phasing in more than 80% of the cases even in complicated ones where selenation was unsuccessful.²³

Furthermore, Tb-Xo4 was also shown to be compatible with micro-seeding, counter-diffusion crystallisation methods and serial crystallography (mesh-and-collect method).²³⁻²⁴ Both $[\text{Na}]_3[\text{Eu}(\text{DPA})_3]$ and Tb-Xo4 complexes are now commercially available and frequently used by the biocrystallographers community to solve the structures of biological macromolecules of interest for nucleation and/or for phasing steps.²⁵⁻³¹ As a consequence, we now have some feedback from several structural biology projects involving state-of-the-art high-throughput protocols (pipetting robots, commercial crystallization kits). Several unexpected results suggest interactions between the lanthanide complexes and the crystallization mixtures that can lead to false positive crystallization results or apparent cooperative behavior favoring the lanthanide complex/protein interaction. In this article, we describe two representative examples of such unexpected results: a false positive hit observed during the crystallisation of the Acriflavine resistant protein B (AcrB) from *Escherichia coli* in the presence of $[\text{Na}]_3[\text{Eu}(\text{DPA})_3]$ and an apparent cooperative behavior in the crystal structure of adenylate kinase (AdkA) from *Methanothermococcus thermolithotrophicus* in the presence of Tb-Xo4. In order to rationalise these results, we explore the behavior of our Ln-based additives in the conventional crystallisation kits with a particular focus on the role of divalent alkaline earth or transition metal dications and evidence detrimental auto-crystallisation processes and trans-metalation reactions.

Results and discussions

The crystallisation of AcrB, whose structure was already described (PDB id code: 2GIF), was performed in the presence and absence of $[\text{Na}]_3[\text{Eu}(\text{DPA})_3]$ using the High-throughput Crystallisation facility (HTXlab, EMBL-Grenoble) with six commercial crystallisation kit (see SI). The drops were regularly inspected to detect the crystallisation events and



study the effect of the lanthanide additive.

Figure 2. Crystallisation drops of AcrB from *E. coli* alone (left) and in the presence of $[\text{Eu}(\text{DPA})_3]_3$. (right) in transmission (a) or under 315 nm irradiation (b).

A typical comparison is reported in the Figure 2; the protein alone precipitates as an amorphous slurry whereas in the presence of $[\text{Eu}(\text{DPA})_3]^{3-}$ exploitable crystals have been obtained that were strongly luminescent under UV-irradiation (Figure 2). However, after analysis, these crystals did not contain any protein and are simply composed of pure $[\text{Eu}(\text{DPA})_3]^{3-}$. Consequently, the self-crystallisation of the lanthanide complex in the presence of the protein represents a typical example of false positive hit hampering practical co-crystallisation experiments with proteins.

On the other hand, the crystallisation trial of proteins from the marine archa *Methanothermococcus thermolithotrophicus* performed in the presence and absence of crystallophore Tb-Xo4 allowed us to solve four protein structures,^{23, 30-31} including AdkA. The problem observed in the case of crystallisation of AcrB with $[\text{Na}]_3[\text{Eu}(\text{DPA})_3]$, such as the self-crystallisation of the lanthanide complex, was not observed. The structure of AdkA (PDB id code: 6HF7) was solved at 1.96 Å resolution in a condition containing 50 mM of magnesium ion.¹⁹ The asymmetric unit contains a homo-trimer (Figure 3a) and two of the four bound Tb-Xo4 molecules with the highest occupancy (0.7) were unambiguously modelled. The two Tb-Xo4 molecules are located at the same site on two AdkA monomers, and involve an identical supramolecular interactions network. The analogous site on third protein monomer is unoccupied due to particular crystal contacts. A detailed investigation of the binding pocket reveals the involvement of a hydrated magnesium dication bridging the crystallophore with the surface protein through aspartate 90 (Figure 3b). The second feature is the presence of a glycerol molecule from the protein buffer, completing the coordination sphere of the terbium ion. Starting from this crystal structure, the main binding site was investigated using DFT calculation (see SI). The strongest interaction involves the hydrated magnesium and the aspartate residue (D90) ensuring the binding of the crystallophore to AdkA surface and corresponding to a global interaction energy of $-25.3 \text{ kcal}\cdot\text{mol}^{-1}$ (Figure S1 and table S1). This unexpected formation of a $\{\text{AdkA}/\text{Tb-Xo4}/\text{Mg}^{2+}/\text{glycerol}\}$ adduct at the surface of the AdkA protein surface is comparable to the recently reported structure of FprA with a $\{\text{FprA}/\text{Tb-Xo4}/\text{Ca}^{2+}/\text{glycerol}\}$ adduct.³² In both cases, a glycerol molecule was also involved near Tb-Xo4. The alkaline-earth cation (Mg^{2+} or Ca^{2+}) as well as glycerol were present in the crystallisation mixture.

The results obtained during the crystallisation of AcrB with $[\text{Na}]_3[\text{Eu}(\text{DPA})_3]$ and the *M. thermolithotrophicus* proteins with Tb-Xo4 prompted us to investigate systematically the behavior of the two complexes with the different constituents of several commercial crystallisation kits (Tables S2, S3) routinely used for automated crystallisation experiments at the HTX lab (EMBL, Grenoble). These kits represent a total of 576 unique conditions varying the pH and nature of the buffer (TRIS, MES, HEPES, citric acid, sodium acetate...), diverse types of salts (NaCl , $(\text{NH}_4)_2\text{SO}_3$, MgCl_2 , CaCl_2 ...) and different precipitants (polyethyleneglycol of various length, methyl-2,4-pentanediol, isopropanol...) at different concentrations. In order to evaluate the behavior of our lanthanide-based additives in such media, the lanthanide complexes were systematically tested alone, one-by-one, in

these conventional crystallisation kits. The experiment was performed by mixing equal volume of the additive solution at the desired concentration (10-100 mM for Tb-Xo4, 25-100 mM for $[\text{Na}]_3[\text{Eu}(\text{DPA})_3]$) with the crystallisation solution to form a sitting drop (Tables S1 and S2). Then, we evaluated the presence of potential lanthanide complexes self-crystallisation or precipitate formation by conventional imaging techniques and the instability of the complexes by the disappearance of the lanthanide emission signal under UV irradiation.

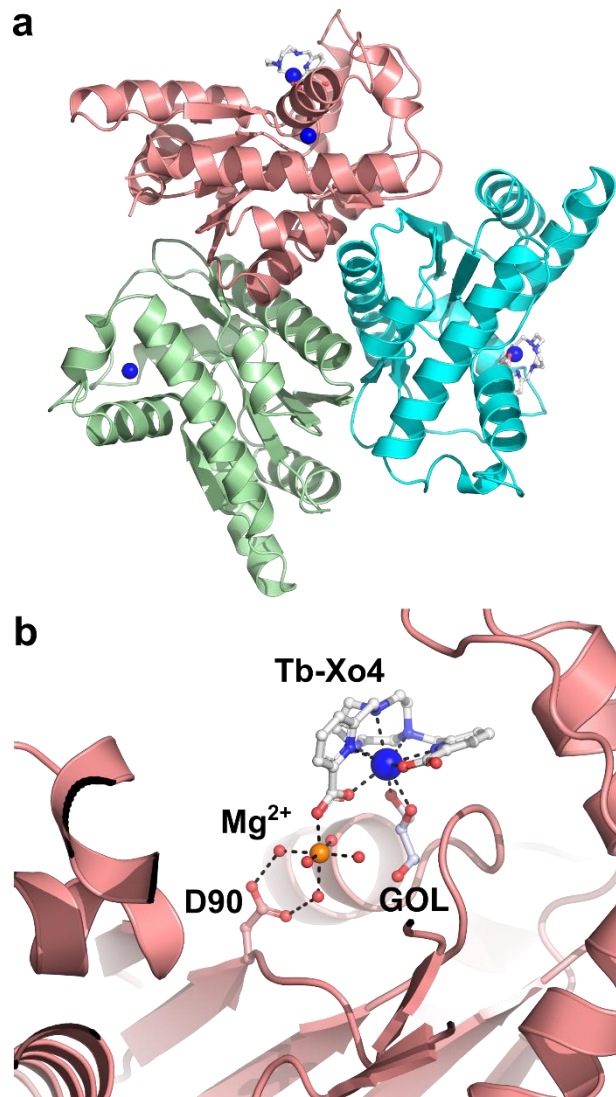
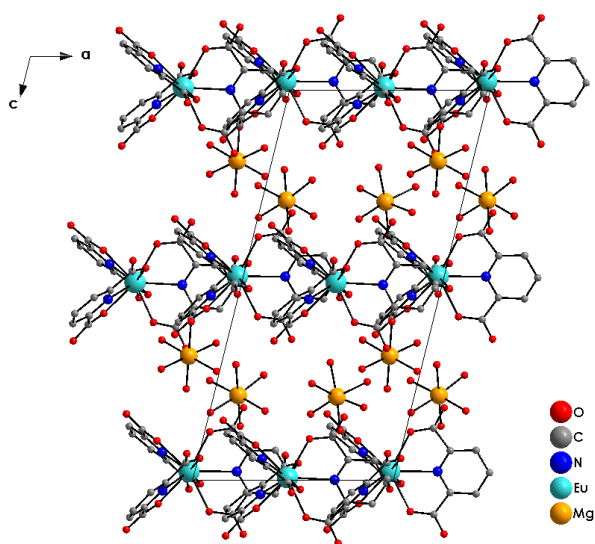


Figure 3. b) Trimer of AdkA from *M. thermolithotrophicus* co-crystallized with Tb-Xo4 (10 mM, Tb^{3+} in blue) in the presence of MgCl_2 ; the three individual AdkA units forming the trimer are represented in salmon, light green and aqua blue. b) Insights into the Tb-Xo4 main binding site. GOL: glycerol, Mg^{2+} in orange, O in red, C in gray and N in blue.

The spontaneous crystallisation of $[\text{Na}]_3[\text{Eu}(\text{DPA})_3]$ was observed in 10% of the conditions at 25 mM and this ratio increased up to 30% at 100 mM. The analysis of these conditions indicated that high concentrations of salt (such as

NaCl, (NH₄)₂SO₃...), typically higher than 0.8 M, the presence of divalent salts (Ca²⁺, Mg²⁺) and 2-methyl-2,4-pentanediol or isopropanol favored the self-crystallisation of the tris-dipicolinate complex. The increase of the anionic strength or the decrease of the solubility of the complex in the presence of alcohol in the media are classical ways to promote crystallisation, in which the effect of divalent cations was less expected. Therefore, the reactions of [Na]₃[Eu(DPA)₃] with each alkaline-earth salts (MgCl₂, CaCl₂ or BaCl₂) were undertaken. The lower solubility of the divalent alkaline earth chloride solutions into an aqueous [Na]₃[Eu(DPA)₃] solution results in the fast formation of transparent crystals, which were almost insoluble in water and organic solvent. Diffraction experiments performed on these crystals revealed the formation of structures of the following compounds (Mg(H₂O)₆)₃[Eu(DPA)₃]₂·7H₂O (1), {(Ca(H₂O)₄)₃



[Eu(DPA)₃]₂]_n·11nH₂O (2) and of the previously reported {[Eu(DPA)₃]₂Ba₃(H₂O)₆]_n·4H₂O}^{33,34-35}

Figure 4. Projection along the b-axis of the unit-cell of the crystal packing of complex 1, (Mg(H₂O)₆)₃[Eu(DPA)₃]₂·7H₂O. For clarity, hydrogen atoms and non-coordinated water molecules have been removed.

Crystal data and refinement parameters are given in Table S4, whereas selected bond lengths are compiled in Tables S5 and S7. In these structures, the Na⁺ counter-ion was completely replaced by Mg²⁺/Ca²⁺/Ba²⁺, respectively, which are coordinated by water or by [Eu(DPA)₃]³⁻ carboxylate forming 3-to-2 assemblies with the complex (Figures 4 and 5). The crystal structures explain the strong decrease of solubility. While the structure of 1 exhibits isolated [Eu(DPA)₃]³⁻ and [Mg(H₂O)₆]²⁺ units (Figure 4), 2 presents a 3D network with [Eu(DPA)₃]³⁻ building blocks connected together through [Ca(H₂O)₆]²⁺ or [Ca(H₂O)₈]²⁺ bridges (Figures 5). In that latter case, an oxygen atom of one (for two ligands) or both (for one ligand) the two DPA carboxy functions complete the Ca²⁺ environment creating links in the three directions between Eu(III) and Ca(II) complexes. The geometric configurations of both complexes were analyzed with the help of SHAPE2.1 program (Tables S6 and S8 for compounds 1 and 2, respectively). Each Eu³⁺ cations environment within 1 and 2 structures fit well with a nona-coordinate capped square antiprism (CSAPR-9, C_{4v}) and a tricapped trigonal prism (TCTPR-9, D_{3h}), in the compounds 1 and 2, respectively. All the Eu-O and Eu-N bond lengths (Tables S5 and S7) are in good agreement with those observed in the literature.³⁶⁻³⁹

During automated crystallisation experiments, we also noticed that the characteristic red emission of [Eu(DPA)₃]³⁻ disappeared systematically for all the formulations containing transition metal ions (with M²⁺ = Cd²⁺, Zn²⁺, Ni²⁺, Fe²⁺, Co²⁺ and mix). Measurements of the [Na]₃[Eu(DPA)₃] emissions were performed in the presence of MCl₂ in diluted water solution ([Ln] = 1 mM, Figure S5). The luminescence of [Na]₃[Eu(DPA)₃] is rapidly quenched after addition of 1 eq. of MCl₂ and about 80% of the emission had disappeared after 60 s.

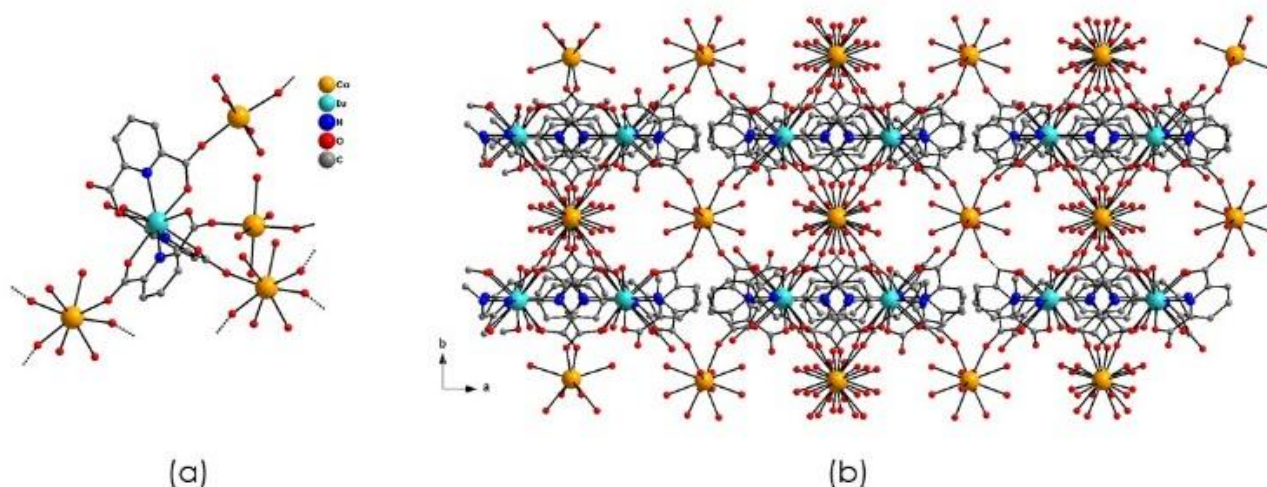


Figure 5. (a) molecular building block of $\{(\text{Ca}(\text{H}_2\text{O})_4)_3[\text{Eu}(\text{DPA})_3]_2\}_n \cdot 11\text{H}_2\text{O}$ complex **2**; (b) projection along the *c*-axis of the unit-cell in order to highlight $[\text{Ca}(\text{H}_2\text{O})_n]^{2+}$ (in orange) and $[\text{Eu}(\text{DPA})_3]^{3-}$ (in blue) planes running perpendicularly to the *b*-axis of the unit-cell. For clarity, hydrogen atoms and non-coordinated water molecules have been removed.

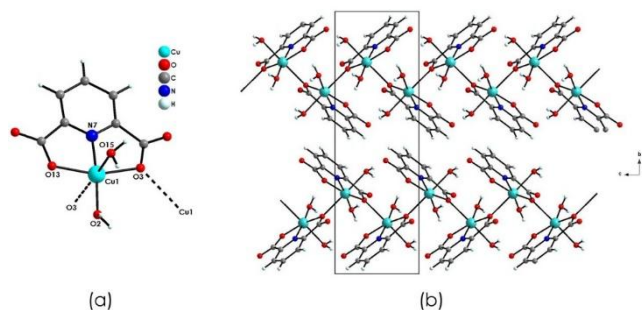


Figure 6. (a) molecular unit of **3** with important labels; (b) projection along the *a*-axis of the unit-cell of $\{\text{Cu}(\text{DPA})(\text{H}_2\text{O})_2\}_n$ chains running along the *c*-axis of the unit-cell.

This competition experiment was also performed at a concentration closer to the crystallisation conditions and the slow diffusion of a CuCl_2 solution (50 mM) in $[\text{Na}]_3[\text{Eu}(\text{DPA})_3]$ (50 mM) led to the formation of crystals of $\{\text{Cu}(\text{DPA})(\text{H}_2\text{O})_2\}_n$ (**3**) suitable for X-rays diffraction analysis (Figure 6, Tables S4 and S9). Cu(II) is coordinated to one deprotonated ligand (via two oxygen and one nitrogen atoms) and two water molecules. The distorted cation octahedral ML_6 {O5N1} environment is then completed by one oxygen atom (O3) belonging to one neighboring complex unit. This bridge leads to the formation of chains of complexes running along the *c*-axis of the unit-cell with a $\text{Cu}^{2+} \dots \text{Cu}^{2+}$ intra-chain distance equals to 3.87 Å. All the Cu-N, Cu-O bond lengths and O-Cu-O, N-Cu-O bond angles (Table S9) are in agreement with those usually listed in the literature for corresponding systems.⁴⁰ $\{\text{Cu}(\text{DPA})(\text{H}_2\text{O})_2\}_n$ chains perfectly stack one above the others in the *a*-direction of the unit-cell and are slightly shifted in the *c*-direction of the unit-cell. Structural cohesion between chains is assumed by weak interactions (hydrogen bonds and Van der Waals interactions). These

results indicated that a transmetalation reaction occurs very rapidly between $[\text{Eu}(\text{DPA})_3]^{3-}$ and transition metal cations leading to the destruction of the lanthanide complex in solution.

The behavior of the Tb-Xo4 complex in the automated crystallisation conditions is completely different with all drops remaining perfectly homogeneous, without any sign of precipitation at 10 mM concentration. At 100 mM, only 3 conditions over 576 led to the formation of micro-crystalline precipitate (Figures S2-4). These conditions contain among other components ammonium fluoride, calcium acetate or ammonium sulfate as well as polyethylene glycol. These microcrystals were not suitable for X-ray diffraction and we were unable to produce larger and better diffracting crystals in these conditions. After several crystallisation attempts, we hardly grew Tb-Xo4 crystals of global formula $[\text{Tb}_4\text{L}_4(\text{H}_2\text{O})_4]\text{Cl}_4 \cdot 15\text{H}_2\text{O}$ (**4**) from slow evaporation of a Tb-Xo4/water/acetonitrile mixture (Tables S4, S10 and S11). These crystals are luminescent in the green upon UV irradiation (Figure 7). In the structure, four Tb-Xo4 complexes assemble in a remarkable tetrameric supramolecular architecture (Figure 7). Each Tb(III) atom is coordinated in a {N5O4} environment. The deprotonated ligand L is coordinated by two oxygen atoms from the carboxylate moieties and five nitrogen ones from the pyridine and the triazacyclononane macrocycle. The Tb-O bond lengths (2.403 Å) are shorter than Tb-N ones (2.566 Å) and are in good agreement with those previously reported in the literature for identical complexes.⁴¹ The coordination sphere is further completed by the two oxygen atoms from one water molecule with Tb-O bond length (2.449 Å) comparable to other Tb-O(L) ones and one oxygen atom from the carbonyl fragment belonging to the ligand of a neighboring complex with a shorter Tb-O bond (2.265 Å). The later interaction forces the positioning of the second complex with a 90° angle in relation to the first one. As all four complexes have the same

environment Tb-Xo4 associates as a square tetramer (Figure 7). The charge is balanced by the presence of four Cl⁻ anions within the unit-cell. Fifteen non-coordinated water molecules also co-crystallize within the unit-cell. Both of these non-coordinated molecules or anions are located in channels running along the c-axis of the unit-cell and generated by the global complexes packing.

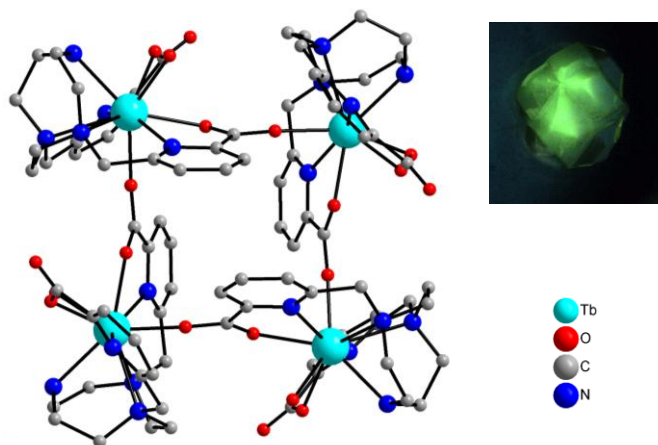


Figure 7. Structure of complex 4. For clarity, hydrogen atoms, non-coordinated chloride and water molecules are omitted. Crystal of complex 4 emitting green light under UV irradiation ($\lambda_{\text{ex}} = 254 \text{ nm}$, inset).

In addition, stability experiments in solution have been performed for the Tb-Xo4 complex, in the same conditions as those done for the $[\text{Na}_3][\text{Eu}(\text{DPA})_3]$ complex. Firstly, addition of 1 equivalent of MCl_2 to a Tb-Xo4 solution led to a much slower decrease of the green luminescence. 80% luminescence decrease occurs over several days (Figure S6) compared to the almost luminescence decrease observed with seconds for $[\text{Na}_3][\text{Eu}(\text{DPA})_3]$ (Figure S5). Secondly, in the presence of alkaline-earth salts (MgCl_2 , CaCl_2 , BaAc_2 1 to 10 equivalents), the luminescence intensity of Tb-Xo4 doesn't vary over up to 100 days (Figure S7) whereas $[\text{Eu}(\text{DPA})_3]^{3-}$ precipitates and/or self-crystallizes. All results indicated that a transmetalation reaction occurs between the two lanthanide complexes and transition metal cations but with a very different kinetic underlining a higher stability for the macrocyclic Tb-Xo4 complex. In addition, in the presence of alkaline-earth salts, Tb-Xo4 is highly stable whereas $[\text{Eu}(\text{DPA})_3]^{3-}$ precipitates and/or self-crystallizes.

Conclusion.

In this article, we analyzed the use of two lanthanide complexes ($[\text{Na}_3][\text{Eu}(\text{DPA})_3]$ and Tb-Xo4) as nucleating agents in two protein crystallization experiments. We discovered that $[\text{Na}_3][\text{Eu}(\text{DPA})_3]$ can self-crystallize and give false positive crystallization hits in particular in the presence of alkaline-earth. We also uncovered a potential interaction between Tb-Xo4 and some chemicals present in protein crystallization kits, leading to the formation of complex adducts such as $\{\text{AdkA/Tb-Xo4/Mg}^{2+}/\text{GOL}\}$ or $\{\text{FprA/Tb-Xo4/Ca}^{2+}/\text{GOL}\}$ at the surface of proteins. We thus analyzed the behavior of the additives alone in the same commercial

crystallization kits. This study reveals that the initial tris-dipicolinate complex presents a lower chemical stability and a strong tendency to self-crystallisation detrimental for its use in high-throughput robotized crystallisation platform. On the other hand, the Tb-Xo4 is perfectly soluble in the crystallisation media, stable in the presence of alkaline-earth dications and slowly decomposed (within days) by transmetalation with transition metals. We therefore recommend to use Tb-Xo4 over $[\text{Na}_3][\text{Eu}(\text{DPA})_3]$ as “protein glue” in HTX crystallization assay. The tris-dipicolinate is better suited for soaking experiments of native crystal in a more controlled medium.

Acknowledgements.

Authors acknowledge the Fondation Maison de la Chimie, Agence Nationale de la Recherche (ANR Ln23-13-BS07-0007-01) and SATT Pulsalys for grants to AR, SE and SDP. The region AuRA is also strongly acknowledged for its financial support (program Xo4-2.0 and Crystfrag granting ZA, AYR and AB respectively). Authors also thank the Polyvalan Company for its help and the pôle de compétitivité Lyon-Biopôle.

Keywords. Protein crystallography • lanthanide complexes • triazacyclononane • crystallophore

References.

1. Terwilliger, T. C.; Stuart, D.; Yokoyama, S., Lessons from Structural Genomics. *Annual Rev. Biophys.* **2009**, *38* (1), 371-383.
2. Khurshid, S.; Saridakis, E.; Govada, L.; Chayen, N. E., Porous nucleating agents for protein crystallisation. *Nat. Protoc.* **2014**, *9* (7), 1621-1633.
3. Khurshid, S.; Saridakis, E.; Govada, L.; Chayen, N. E., Porous nucleating agents for protein crystallisation. *Nat Protoc* **2014**, *9* (7), 1621-33.
4. Santarsiero, B. D.; Yegian, D. T.; Lee, C. C.; Spraggon, G.; Gu, J.; Scheibe, D.; Uber, D. C.; Cornell, E. W.; Nordmeyer, R. A.; Kolbe, W. F.; Jin, J.; Jones, A. L.; Jaklevic, J. M.; Schultz, P. G.; Stevens, R. C., An approach to rapid protein crystallisation using nanodroplets. *J. Appl. Crystallogr.* **2002**, *35*, 278-281.
5. Brown, J.; Walter, T. S.; Carter, L.; Abrescia, N. G. A.; Aricescu, A. R.; Batuwangala, T. D.; Bird, L. E.; Brown, N.; Chamberlain, P. P.; Davis, S. J.; Dubinina, E.; Endicott, J.; Fennelly, J. A.; Gilbert, R. J. C.; Harkiolaki, M.; Hon, W. C.; Kimberley, F.; Love, C. A.; Mancini, E. J.; Manso-Sancho, R.; Nichols, C. E.; Robinson, R. A.; Sutton, G. C.; Schueller, N.; Sleeman, M. C.; Stewart-Jones, G. B.; Vuong, M.; Welburn, J.; Zhang, Z.; Stammers, D. K.; Owens, R. J.; Jones, E. Y.; Harlos, K.; Stuart, D. I., A procedure for setting up high-throughput nanolitre crystallisation experiments. II. Crystallisation results. *J. Appl. Crystallogr.* **2003**, *36*, 315-318.
6. Hendrickson, W. A., Anomalous diffraction in crystallographic phase evaluation. *Rev. Biophys.* **2014**, *47* (1), 49-93.
7. Doublé, S., Preparation of selenomethionyl proteins for phase determination. In *Methods Enzymol.*, Academic Press: 1997; Vol. 276, pp 523-530.
8. D'Arcy, A.; Mac Sweeney, A.; Haber, A., Using natural seeding material to generate nucleation in protein crystallisation experiments. *Acta Crystallogr. Section D-Biol. Crystallogr.* **2003**, *59*, 1343-1346.
9. Georgieva, D. G.; Kuil, M. E.; Oosterkamp, T. H.; Zandbergen, H. W.; Abrahams, J. P., Heterogeneous nucleation of three-dimensional protein nanocrystals. *Acta Crystallogr. Section D-Biol. Crystallogr.* **2007**, *63*, 564-570.

10. Saridakis, E.; Khurshid, S.; Govada, L.; Phan, Q.; Hawkins, D.; Crichlow, G. V.; Lolis, E.; Reddy, S. M.; Chayen, N. E., Protein crystallisation facilitated by molecularly imprinted polymers. *Proc. Nat. Ac. Sci.* **2011**, *108* (27), 11081.
11. Khurshid, S.; Govada, L.; El-Sharif, H. F.; Reddy, S. M.; Chayen, N. E., Automating the application of smart materials for protein crystallisation. *Acta Crystallogr. Section D-Struct.Biol.* **2015**, *71*, 534-540.
12. Bijelic, A.; Rompel, A., The use of polyoxometalates in protein crystallography - An attempt to widen a well-known bottleneck. *Coord. Chem. Rev.* **2015**, *299*, 22-38.
13. Breibeck, J.; Bijelic, A.; Rompel, A., Transition metal-substituted Keggin polyoxotungstates enabling covalent attachment to proteinase K upon co-crystallisation. *Chem Commun* **2019**, *55* (77), 11519-11522.
14. Mac Sweeney, A.; Chambovey, A.; Wicki, M.; Muller, M.; Artico, N.; Lange, R.; Bijelic, A.; Breibeck, J.; Rompel, A., The crystallisation additive hexatungstotellurate promotes the crystallisation of the HSP70 nucleotide binding domain into two different crystal forms. *PLoS One* **2018**, *13* (6), e0199639.
15. Bijelic, A.; Rompel, A., Polyoxometalates: more than a phasing tool in protein crystallography. *ChemTexts* **2018**, *4* (3), 10.
16. McGovern, R. E.; Fernandes, H.; Khan, A. R.; Power, N. P.; Crowley, P. B., Protein camouflage in cytochrome c-calixarene complexes. *Nat Chem* **2012**, *4* (7), 527-33.
17. McGovern, R. E.; Feifel, S. C.; Lisdat, F.; Crowley, P. B., Microscale Crystals of Cytochrome c and Calixarene on Electrodes: Interprotein Electron Transfer between Defined Sites. *Angew. Chem. Int. Ed.* **2015**, *54* (21), 6356-9.
18. Guagnini, F.; Antonik, P. M.; Rennie, M. L.; O'Byrne, P.; Khan, A. R.; Pinalli, R.; Dalcanale, E.; Crowley, P. B., Cucurbit[7]uril-Dimethyllysine Recognition in a Model Protein. *Angew. Chem., Int. Ed.* **2018**, *57* (24), 7126-7130.
19. Engilberge, S.; Rennie, M. L.; Dumont, E.; Crowley, P. B., Tuning Protein Frameworks via Auxiliary Supramolecular Interactions. *ACS Nano* **2019**, *13* (9), 10343-10350.
20. Pompidor, G.; D'Aleo, A.; Vicat, J.; Toupet, L.; Giraud, N.; Kahn, R.; Maury, O., Protein crystallography through supramolecular interactions between a lanthanide complex and arginine. *Angew. Chem. Int. Ed.* **2008**, *47* (18), 3388-91.
21. Talon, R.; Kahn, R.; Dura, M. A.; Maury, O.; Vellieux, F. M.; Franzetti, B.; Girard, E., Using lanthanoid complexes to phase large macromolecular assemblies. *J Synchrotron Radiat* **2011**, *18* (1), 74-8.
22. Engilberge, S.; Riobe, F.; Di Pietro, S.; Lassalle, L.; Coquelle, N.; Arnaud, C. A.; Pitrat, D.; Mulatier, J. C.; Madern, D.; Breyton, C.; Maury, O.; Girard, E., Crystallophore: a versatile lanthanide complex for protein crystallography combining nucleating effects, phasing properties, and luminescence. *Chem Sci* **2017**, *8* (9), 5909-5917.
23. Engilberge, S.; Wagner, T.; Santoni, G.; Breyton, C.; Shima, S.; Franzetti, B.; Riobe, F.; Maury, O.; Girard, E., Protein crystal structure determination with the crystallophore, a nucleating and phasing agent. *J. Appl. Crystallogr.* **2019**, *52* (Pt 4), 722-731.
24. de Wijn, R.; Hennig, O.; Roche, J.; Engilberge, S.; Rollet, K.; Fernandez-Millan, P.; Brillet, K.; Betat, H.; Morl, M.; Roussel, A.; Girard, E.; Mueller-Dieckmann, C.; Fox, G. C.; Olieric, V.; Gavira, J. A.; Lorber, B.; Sauter, C., A simple and versatile microfluidic device for efficient biomacromolecule crystallisation and structural analysis by serial crystallography. *IUCrJ* **2019**, *6* (Pt 3), 454-464.
25. Rempel, S.; Colucci, E.; de Gier, J. W.; Guskov, A.; Slotboom, D. J., Cysteine-mediated decyanation of vitamin B12 by the predicted membrane transporter BtuM. *Nat. Comm.* **2018**, *9* (1), 3038.
26. Hajj Chehade, M.; Pelosi, L.; Fyfe, C. D.; Loiseau, L.; Rascalou, B.; Brugière, S.; Kazemzadeh, K.; Vo, C.-D.-T.; Ciccone, L.; Aussel, L.; Couté, Y.; Fontecave, M.; Barras, F.; Lombard, M.; Pierrel, F., A Soluble Metabolite Synthesizes the Isoprenoid Lipid Ubiquinone. *Cell Chem. Biol.* **2019**, *26* (4), 482-492.e7.
27. Roche, J.; Girard, E.; Mas, C.; Madern, D., The archaeal LDH-like malate dehydrogenase from *Ignicoccus islandicus* displays dual substrate recognition, hidden allostery and a non-canonical tetrameric oligomeric organization. *J. Struct. Biol.* **2019**, *208* (1), 7-17.
28. Schada von Borzyskowski, L.; Severi, F.; Krüger, K.; Hermann, L.; Gilardet, A.; Sippel, F.; Pommerenke, B.; Claus, P.; Cortina, N. S.; Glatter, T.; Zauner, S.; Zarzycki, J.; Fuchs, B. M.; Bremer, E.; Maier, U. G.; Amann, R. I.; Erb, T. J., Marine Proteobacteria metabolize glycolate via the β -hydroxyaspartate cycle. *Nature* **2019**, *575* (7783), 500-504.
29. Belot, L.; Ouldali, M.; Roche, S.; Legrand, P.; Gaudin, Y.; Albertini, A. A., Crystal structure of Mokola virus glycoprotein in its post-fusion conformation. *PLOS Pathogens* **2020**, *16* (3), e1008383.
30. Bernhardsgrütter, I.; Vögeli, B.; Wagner, T.; Peter, D. M.; Cortina, N. S.; Kahnt, J.; Bange, G.; Engilberge, S.; Girard, E.; Riobé, F.; Maury, O.; Shima, S.; Zarzycki, J.; Erb, T. J., The multicatalytic compartment of propionyl-CoA synthase sequesters a toxic metabolite. *Nat. Chem. Biol.* **2018**, *14* (12), 1127-1132.
31. Vogeli, B.; Engilberge, S.; Girard, E.; Riobe, F.; Maury, O.; Erb, T. J.; Shima, S.; Wagner, T., Archaeal acetoacetyl-CoA thiolase/HMG-CoA synthase complex channels the intermediate via a fused CoA-binding site. *Proc Natl Acad Sci* **2018**, *115* (13), 3380-3385.
32. Engilberge, S.; Riobe, F.; Wagner, T.; Di Pietro, S.; Breyton, C.; Franzetti, B.; Shima, S.; Girard, E.; Dumont, E.; Maury, O., Unveiling the Binding Modes of the Crystallophore, a Terbium-based Nucleating and Phasing Molecular Agent for Protein Crystallography. *Chem. Eur. J.* **2018**, *24* (39), 9739-9746.
33. Zhao, X.-Q.; Zuo, Y.; Gao, D.-L.; Zhao, B.; Shi, W.; Cheng, P., Syntheses, Structures, and Luminescence Properties of a Series of LnIII-BallHeterometal-Organic Frameworks. *Cryst. Growth & Des.* **2009**, *9* (9), 3948-3957.
34. Chen, Y.; Li, L.; Zhang, Q.; Liu, S.; Tian, Z.; Ju, Z., Effects of calcium ions on crystal structure and luminescence properties of six rare earth metal complexes. *J. Solid State Chem.* **2020**, *281*, 121053.
35. Chen, Y.; Zhao, X.; Gao, R.; Ruan, Z.; Lin, J.; Liu, S.; Tian, Z.; Chen, X., Temperature-induced solvent assisted single-crystal-to-single-crystal transformation of Mg(II)-Ln(III) heterometallic coordination polymers. *J. Solid State Chem.* **2020**, *292*, 121674.
36. Tancrez, N.; Feuvrie, C.; Ledoux, I.; Zyss, J.; Toupet, L.; Le Bozec, H.; Maury, O., Lanthanide Complexes for Second Order Nonlinear Optics: Evidence for the Direct Contribution of f Electrons to the Quadratic Hyperpolarizability. *J. Am. Chem. Soc.* **2005**, *127* (39), 13474-13475.
37. D'Aléo, A.; Pompidor, G.; Elena, B.; Vicat, J.; Baldeck, P. L.; Toupet, L.; Kahn, R.; Andraud, C.; Maury, O., Two-photon microscopy and spectroscopy of lanthanide bioprobes. *Chemphyschem* **2007**, *8* (14), 2125-32.
38. D'Aléo, A.; Toupet, L.; Rigaut, S.; Andraud, C.; Maury, O., Guanidinium as powerful cation for the design of lanthanate tris-dipicolinate crystalline materials: Synthesis, structure and photophysical properties. *Opt. Mater.* **2008**, *30* (11), 1682-1688.
39. Mooibroek, T. J.; Gamez, P.; Pevec, A.; Kasunic, M.; Kozlevcar, B.; Fu, W. T.; Reedijk, J., Efficient, stable, tunable, and easy to synthesize, handle and recycle luminescent materials: [H₂NMe₂]₂[Ln(III)(2,6-dipicolinate)₃] (Ln = Eu, Tb, or its solid solutions). *Dalton Trans* **2010**, *39* (28), 6483-7.
40. Sileo, E. E.; Rigotti, G.; Rivero, B. E.; Blesa, M. A., Kinetic study of the thermal dehydration of copper(II) dipicolinates: Crystal and molecular structure of Cu(II) (Pyridine 2,6-Dicarboxylato) DI- and Trihydrated. *J. Phys. Chem. Solids* **1997**, *58* (7), 1127-1135.

41. Nocton, G.; Nonat, A.; Gateau, C.; Mazzanti, M., Water Stability and Luminescence of Lanthanide Complexes of Tripodal Ligands Derived from 1,4,7-Triazacyclononane: Pyridinecarboxamide versus Pyridinecarboxylate Donors. *Helv. Chim. Acta* **2009**, 92 (11), 2257-2273.